

Numerical reconstruction of Schrödinger equations with quadratic nonlinearities

Khaoula El Maddah¹, Matti Lassas², and Teemu Tyni¹

¹Research Unit of Applied and Computational Mathematics,
University of Oulu, Finland

²Department of Mathematics and Statistics, University of Helsinki,
Finland

Abstract

We introduce a numerical framework for reconstructing the potential in two dimensional semilinear elliptic PDEs with power type nonlinearities from the nonlinear Dirichlet to Neumann map. By applying higher order linearization method, we compute the Fourier data of the unknown potential and then invert it to recover q . Numerical experiments show accurate reconstructions for both smooth and discontinuous test cases.

1 Introduction

In this paper, we study the semilinear elliptic model

$$-\Delta u + q u^p = 0 \quad \text{in } \Omega, \quad u|_{\partial\Omega} = f, \quad (1)$$

with $p \in \mathbb{N}_{\geq 2}$ on a bounded domain $\Omega \subset \mathbb{R}^n$ and Dirichlet data f . Our objective is to recover the unknown potential $q = q(x)$ from boundary measurements associated with (1). We study this numerically by using the higher order linearization framework of [22] for Calderón type semilinear equations with power nonlinearities. The key idea is to exploit higher derivatives of the nonlinear Dirichlet-to-Neumann (DN) map to obtain auxiliary linearized equations, thereby enabling recovery in settings where the corresponding linear inverse problem is difficult to resolve. In particular, [22] shows that, given the nonlinear DN map, one can simultaneously determine a potential and the underlying conformal manifold in two dimensions, and recover a potential on transversally anisotropic manifolds in dimensions $n \geq 3$. In the Euclidean case, the method yields a notably simple solution to the Calderón problem for certain semilinear equations, without relying on complex geometrical optics (CGO) constructions.

We numerically implement the higher order linearization method for elliptic equations with power type nonlinearities based on the method detailed in [22, 24]. The equation (1) is well-posed for boundary values $f \in C^{2,\alpha}(\partial\Omega)$, and the boundary measurements are encoded by the nonlinear (DN) map

$$\Lambda_q : f \mapsto \partial_\nu u|_{\partial\Omega},$$

which assigns to each boundary value its corresponding normal flux. By evaluating higher Fréchet derivatives of Λ_q , we can obtain an Alessandrini-type integral identity

$$p! \int_{\Omega} q v_0 v^p \, dx = \frac{d^p}{d\varepsilon^p} \int_{\partial\Omega} v_0 \Lambda_q(\varepsilon f) \, dS.$$

Particularly, it suffices to use measurements of the nonlinear functional $\psi : C^{2,\alpha}(\partial\Omega) \rightarrow \mathbb{C}$ given by

$$\psi : f \mapsto \int_{\partial\Omega} \Lambda_q(f) \, dS_x,$$

rather than the full DN-map. By suitable choice of boundary values f , this integral identity produces the Fourier transform of the unknown potential q . Regularized Fourier inversion is then implemented to recover q from noisy and band-limited data as a solution to a regularized least squares problem (Tikhonov or total variation, depending on the expected regularity of q). The methodology applies to any integer power nonlinearity $p \in \mathbb{N}_{\geq 2}$, but we concentrate on the case $p = 2$ for simplicity.

In this work we present, to the best of our knowledge, the first numerical implementation of the higher order linearization method for elliptic nonlinear PDEs. For the forward problem, we propose a discretization scheme for the nonlinear equation (1). For the inverse problem, we design and analyze regularization strategies that combine Savitzky-Golay smoothing for differentiating the noisy data with an isotropic Fourier inversion based on Tikhonov or total variation regularization. The overall reconstruction pipeline is validated through numerical experiments on a range of test configurations, demonstrating the robustness of the method with respect to noise, discretization parameters, and model variations.

For the classical (linear) Schrödinger Calderón problem, several results establish uniqueness and reconstruction under progressively weaker regularity. In two dimensions, Nachman [26] gave a constructive solution for conductivities (potentials) in $W^{2,p}$ using $\bar{\partial}$ (D-bar) techniques, giving an explicit reconstruction formula. Nachman also addressed anisotropic formulation in domains of \mathbb{R}^n , and solve it for C^3 matrix valued potentials. The planar result was later sharpened by Astala-Päivärinta [1], who proved global uniqueness for bounded conductivities, relying on CGO methods and removing the earlier smoothness assumptions. For higher-dimensional results ($n \geq 3$), we refer to Sylvester-Uhlmann [40] and, more recently, Carstea [5]. Other results for Calderón problem on Lipschitz domains, under the assumption that the conductivity belongs to $W^{1,\infty}(\bar{\Omega})$, were established by Tataru and Haberman [12]. These results were improved in [3, 4], where the regularity assumptions were weakened to require only the boundedness and the Lipschitz continuity of the conductivity and where explicit reconstruction formulas were also provided.

Over the past decade, nonlinear inverse problems have progressed rapidly [41], driven by the realization that nonlinear interactions can be exploited as information rather than an obstacle. In the parabolic setting, Isakov [13] showed that the first linearization of the nonlinear Dirichlet to Neumann (DN) map coincides with the DN map of a suitable linear equation, thereby enabling the use of linear inverse theory. For the semilinear Schrödinger equation $\Delta u + a(x, u) = 0$, recovery of the nonlinearity was established in 2D [14, 38] and in higher dimensions [15]. More recently, Johansson-Nurminen-Salo [16, 17] proved that, in a neighborhood of a fixed background solution, the entire nonlinearity $a(x, u)$ is determined from boundary

data, up to the natural gauge. The key method often termed higher order linearization has since become a general tool, with parallel developments for nonlinear elliptic models (including power type semilinear equations [11, 20, 24]), quasilinear equations [18, 37, 39], the degenerate p -Laplace equation [2, 32], and and fractional semilinear Schrödinger problems [21].

Similar equations of the form (1), often in more complex settings, arise in a variety of applications (e.g., steady states of reaction diffusion systems with power type kinetics [29, 36], population dynamics with nonlinear birth/death terms [25, 27] and combustion and Emden–Fowler type models [6, 9, 10]), where $q(x)$ encodes spatial heterogeneity and $p > 1$ the order of the nonlinearity. Despite substantial theoretical progress, numerical implementations for nonlinear elliptic inverse problems remain comparatively limited; our work takes a step in that direction.

The paper is organized as follows. In Section 2 we explicit the higher order linearization method for the semilinear elliptic equation (1), as explained in [22]. Section 3 details the Newton framework used to solve the forward numerical problem using FEM. Section 4 focuses on the reconstruction of the potential: We first recover Fourier data by applying the higher order linearization method to the quadratic case $p = 2$ (Section 2), then we specify the choice of the boundary conditions (Section 4.1); next, we derive a matrix formulation of the problem (Section 4.2); finally, we invert the Fourier transform and reconstruct q from noisy measurements (Section 4.3). Section 5 presents numerical experiments. The appendices contain supporting material: Appendix A justifies the convergence of Newton method; and Appendix B discusses regularized higher order differentiation using Savitzky-Golay filter via local polynomial regression.

2 Higher order linearization method for the semilinear elliptic equation

Let $\Omega \subset \mathbb{R}^n$ be a bounded domain with smooth boundary $\partial\Omega$. We consider the semilinear elliptic boundary value problem

$$\begin{cases} -\Delta u_\varepsilon + q u_\varepsilon^p = 0, & \text{in } \Omega, \\ u_\varepsilon|_{\partial\Omega} = \sum_{j=1}^m \varepsilon_j f_j, & \text{on } \partial\Omega \end{cases} \quad (2)$$

where $\varepsilon = (\varepsilon_1, \dots, \varepsilon_m) \in \mathbb{R}^m$ are small parameters and $f_j \in C^{2,\alpha}(\partial\Omega)$, with $0 < \alpha < 1$, are prescribed boundary data. Below, the function $q \in C^\alpha(\Omega, \mathbb{R})$ is called the potential function. For sufficiently small ε equation (2) admits a unique small solution $u_\varepsilon \in C^{2,\alpha}(\Omega)$, see [22]. Moreover, it can be shown that the solution map $S : C^{2,\alpha}(\partial\Omega) \supset B_\varepsilon(0) \rightarrow C^{2,\alpha}(\Omega)$, $S(f) = u_f$, mapping the boundary value $f \in B_\varepsilon(0) := \{g \in C^{2,\alpha}(\partial\Omega) \mid \|g\|_{C^{2,\alpha}(\partial\Omega)} \leq \varepsilon\}$ to the corresponding solution of (2), is C^∞ -map in the Fréchet sense in the neighbourhood of the origin in $C^{2,\alpha}(\partial\Omega)$. This justifies the differentiation of (2) with respect to the small parameters ε_j , and in the sequel we will understand any (partial) derivatives of u_ε with respect to ε to mean Fréchet derivatives of the solution map S .

Next, let us denote

$$v_j := \left. \frac{\partial u_\varepsilon}{\partial \varepsilon_j} \right|_{\varepsilon=0}.$$

Then differentiating (2) with respect to ε_j and evaluating at $\varepsilon_1 = \dots = \varepsilon_m = 0$ yields

$$-\Delta v_j = 0 \quad \text{in } \Omega, \quad v_j|_{\partial\Omega} = f_j,$$

Thus, each v_j is a harmonic function independent of q . Let then $\sigma = (\sigma_1, \dots, \sigma_m)$ be a multi-index with $|\sigma| = p$ and define

$$w := D_{\varepsilon_1, \dots, \varepsilon_m}^\sigma u_\varepsilon \Big|_{\varepsilon_1 = \dots = \varepsilon_m = 0} = \frac{\partial^{\sigma_1}}{\partial \varepsilon_1^{\sigma_1}} \cdots \frac{\partial^{\sigma_m}}{\partial \varepsilon_m^{\sigma_m}} u_{\varepsilon_1, \dots, \varepsilon_m} \Big|_{\varepsilon_1 = \dots = \varepsilon_m = 0}.$$

Differentiating equation (2) p times with respect to $\varepsilon_1, \dots, \varepsilon_m$ and evaluating at $\varepsilon_1 = \dots = \varepsilon_m = 0$, we obtain the linear problem

$$\begin{cases} -\Delta w + p! q \prod_{i=1}^m v_i^{\sigma_i} = 0, & \text{in } \Omega, \\ w = 0, & \text{on } \partial\Omega. \end{cases} \quad (3)$$

Equation (3) shows that the p -th order linearization w solves a linear elliptic PDE with source term given by $q(x)$ times a product of harmonic functions v_j .

Finally, to obtain a useful integral identity, we let $v_0 \in H^1(\Omega)$ be any harmonic function;

$$-\Delta v_0 = 0 \quad \text{in } \Omega.$$

Multiplying (3) by v_0 and integrating by parts yields

$$p! \int_{\Omega} q v_0 \prod_{i=1}^m v_i^{\sigma_i} dx = \int_{\partial\Omega} f_0 \partial_\nu w dS, \quad (4)$$

where $f_0 := v_0|_{\partial\Omega}$ and ∂_ν denotes the outward normal derivative on $\partial\Omega$. The right-hand side of (4) is determined by the Dirichlet-to-Neumann map of the nonlinear problem. Hence, knowledge of the DN map determines the integrals

$$\int_{\Omega} q v_0 \prod_{i=1}^m v_i^{\sigma_i} dx,$$

for arbitrary choices of boundary data $\{f_j\}$ and harmonic test functions v_0 . This provides the key identity for recovering the potential q from the boundary measurements.

3 Numerical solution of the Nonlinear Schrödinger equation

We consider the nonlinear boundary value problem

$$\begin{cases} -\Delta u + q u^p = 0 & \text{in } \Omega, \\ u = f & \text{on } \partial\Omega, \end{cases} \quad (5)$$

where $\Omega \subset \mathbb{R}^d$ is a bounded domain, $p \in \mathbb{N}_{\geq 2}$ the power of the nonlinearity, $q \in C^\alpha(\Omega, \mathbb{R})$ is a given potential function, and $f \in C^{2,\alpha}(\partial\Omega, \mathbb{C})$ prescribes the Dirichlet boundary conditions. The nonlinearity in (5) makes the problem nontrivial to solve numerically. We adopt a Newton-type approach applied to its variational formulation. For this purpose, let $V = \{u \in H^1(\Omega, \mathbb{C}) \mid u|_{\partial\Omega} = f\}$ and

$$V_0 := H_0^1(\Omega) = \{v \in H^1(\Omega, \mathbb{C}) \mid v|_{\partial\Omega} = 0\}.$$

Multiplying (5) by a test function $v \in V_0$ and integrating by parts, we obtain the weak formulation: find $u \in V$ such that

$$F(u)(v) := \int_{\Omega} \nabla u \cdot \overline{\nabla v} \, dx + \int_{\Omega} q(x) u^p \bar{v} \, dx = 0, \quad \forall v \in V_0. \quad (6)$$

Here \bar{z} denotes the complex conjugate of $z \in \mathbb{C}$. Therefore $F(u)(v)$ is a nonlinear functional in u that vanishes at the solution. It can be noted that for each fixed $u \in V$ the conjugate linear functional $F(u) : V_0 \rightarrow \mathbb{C}$ is bounded; the proof is included in Appendix A, as the argument is standard.

To solve (6), we apply Newton's method. Given an iterate $u_n \in V$, we seek an increment $\delta u \in V_0$ such that

$$DF(u_n)[\delta u; v] = -F(u_n)(v), \quad \forall v \in V_0, \quad (7)$$

where $DF(u_n)$ denotes the Fréchet derivative of F with respect to u , evaluated at u_n . Computing this derivative, we obtain the Jacobian sesquilinear form

$$DF(u_n)[\delta u; v] = J(u_n; \delta u, v) = \int_{\Omega} \nabla \delta u \cdot \overline{\nabla v} \, dx + \int_{\Omega} pq(x) u_n^{p-1} \delta u \bar{v} \, dx. \quad (8)$$

It can be verified (see Appendix A) that for a fixed and sufficiently small $u_n \in H^1(\Omega)$, the Jacobian J is a bounded and coercive sesquilinear form on $V_0 \times V_0$. By the Lax-Milgram theorem, it is therefore invertible as an operator from V_0 to V_0' and the linearized problem (7) admits a unique solution $\delta u \in V_0$.

Thus, the Newton step consists of solving the linearized problem (7) with the Jacobian (8), and updating

$$u_{n+1} = u_n + \delta u.$$

The iterations are repeated until convergence, typically monitored by the residual norm

$$\|F(u_n)\|_{V_0'} < \varepsilon_{\text{tol}}$$

for a prescribed tolerance $\varepsilon_{\text{tol}} > 0$. This procedure ensures quadratic convergence (see [19], [28]), provided the initial guess u_0 is sufficiently close to the solution u , and the Jacobian remains coercive through the iteration.

Theorem 3.1 (Well-posedness of the Newton step and convergence). *Let $F : V \rightarrow V_0'$ be the nonlinear residual associated with the boundary value problem (5) on a smooth bounded domain Ω , with V and V_0 as defined above.*

(i) *If u_n is sufficiently close to the exact solution u , then the linearized problem*

$$DF(u_n)[\delta u] = -F(u_n) \quad \text{in } V_0'$$

admits a unique solution $\delta u \in V_0$.

(ii) *If the initial guess $u_0 \in V$ is sufficiently close to u , the Newton iteration*

$$u_{n+1} = u_n + \delta u_n, \quad \delta u_n \text{ solving the linearized step,}$$

is well defined and converges to u in V .

Implementation notes In practice, this method is implemented in a finite element framework. At each Newton iteration, a linear system is assembled from the Jacobian and the residual, and subsequently solved. The nonlinearity enters both the residual and the Jacobian, so care must be taken to update these at each step. In our implementation, the Python-based FEniCX environment handles the automatic differentiation of the variational form to compute the Jacobian (see [31], [8]).

For the numerical simulations 5, the nonlinear Schrödinger equation is discretized using a conforming finite element method on a circular domain $\Omega = \{x \in \mathbb{R}^2 : |x| \leq 1\}$. The mesh is generated from a quasi-uniform triangulation of the disk obtained from a radial resolution of 64 points, corresponding to an average mesh size $h \approx \frac{2}{64} \simeq 3.1 \times 10^{-2}$. The solution is approximated in a Lagrange P_3 finite element space. The nonlinear system is solved using Newton method with a residual based stopping criterion and a relative tolerance of 10^{-8} . For all simulations, Newton's method converges in a small number of iterations (typically between 2 and 3 iterations), compared to a typical Banach fixed-point iteration, which can take 25–35 steps.

4 Reconstruction of the potential

In this section we present the theoretical framework for reconstructing the potential q in the nonlinear equation (1) with $p = 2$. In Section 2, we applied a higher order linearization; with a suitable choice of boundary data see Section 4.1 this returns explicitly the Fourier transform $\mathcal{F}(q)$. Section 4.2 then develops a discretized formulation of the inverse problem, and Section 4.3 describes its numerical solution via Tikhonov or total-variation (TV) regularization, selected according to the expected smoothness of q .

We consider the nonlinear boundary-value problem

$$\begin{cases} -\Delta u + q u^2 = 0, & \text{in } \Omega, \\ u = \varepsilon f, & \text{on } \partial\Omega. \end{cases} \quad (9)$$

As in Section 2, let us denote

$$v = \left. \frac{\partial u}{\partial \varepsilon} \right|_{\varepsilon=0}, \quad w = \left. \frac{\partial^2 u}{\partial \varepsilon^2} \right|_{\varepsilon=0}.$$

By applying higher order linearization method (see Section 2 with $p = 2$ in (4)), we have the integral identity:

$$\int_{\partial\Omega} f_0 \partial_\nu w \, ds = 2 \int_{\Omega} q v^2 v_0 \, dx. \quad (10)$$

Remark 4.1. Note that for the purpose of numerical simulations it is possible to use the identity

$$\langle \Lambda_q(f), f_0 \rangle_{\partial\Omega} = \int_{\Omega} q u^2 v_0 \, dx, \quad (11)$$

to get an easier way to evaluate the left hand side of the equation (10) as

$$\int_{\partial\Omega} v_0 \partial_\nu w \, ds = \frac{\partial^2}{\partial \varepsilon^2} \int_{\Omega} v_0 q u^2 \, dx. \quad (12)$$

Indeed, in simulations one could use the right-hand side of (12) as the synthetic data. The benefit here is that one does not need to numerically compute the normal derivative of u on the boundary $\partial\Omega$, rather the integrals of v_0qu^2 over Ω suffice as the data.

4.1 Choice of the harmonic functions and boundary values

There are many possible ways to choose the auxiliary function v_0 and the boundary value f . A first choice might be to select v_0 and f so that we have the Calderón's exponentials

$$v_0(x) = e^{(-\zeta-i\xi)\cdot x/2}, \quad v(x) = e^{(\zeta-i\xi)\cdot x/4},$$

where $|\xi| = |\zeta|$ and $\xi \cdot \zeta = 0$. Let us denote $f_0 := v_0|_{\partial\Omega}$. Then from (12) we obtain

$$\frac{\partial^2}{\partial\varepsilon^2} \int_{\partial\Omega} f_0 \Lambda_q(\varepsilon f) \, ds \Big|_{\varepsilon=0} = 2 \int_{\Omega} q(x) e^{-i\xi\cdot x} \, dx. \quad (13)$$

By Fourier inversion, this provides an explicit reconstruction formula for the potential q given measurements of Λ_q .

Instead of varying v_0 , we opt to use combinations of boundary values of $f_{\pm} = (v_1 \pm v_2)|_{\partial\Omega}$, which yields two corresponding solutions u_+ and u_- . Then the following algebraic identity holds:

$$(v_1 + v_2)^2 - (v_1 - v_2)^2 = 4v_1v_2.$$

Here, the choice of Calderón exponentials

$$v_1(x) = \frac{1}{2}e^{(-\zeta-i\xi)\cdot x/2} \quad \text{and} \quad v_2(x) = \frac{1}{2}e^{(\zeta-i\xi)\cdot x/2}$$

yields

$$v_1v_2 = \frac{1}{4}e^{-i\xi\cdot x}.$$

Therefore, if we can obtain the *two* measurements (for each ξ):

$$\frac{d^2}{d\varepsilon^2} \int_{\partial\Omega} f_0 \Lambda_q(\varepsilon f_{\pm}) \, ds \Big|_{\varepsilon=0} = 2 \int_{\Omega} qv_0(v_1 \pm v_2)^2 \, dx$$

their difference produces

$$\frac{d^2}{d\varepsilon^2} \int_{\partial\Omega} v_0 \Lambda_q(\varepsilon(f_+ - f_-)) \, ds \Big|_{\varepsilon=0} = 2 \int_{\Omega} 4qv_0v_1v_2 \, dx = 2 \int_{\Omega} q(x) e^{-i\xi\cdot x} \, dx, \quad (14)$$

where we chose $v_0 \equiv 1$ (compare the LHS to (13)).

This latter choice of boundary values f_{\pm} is motivated physically: suppose there is a measurement device, which for each input f simply integrates the boundary value $\partial_\nu u|_{\partial\Omega}$ and returns a complex number. We *do not need to know the full DN-map* (operator), rather it suffices to measure the functional $\psi : C^{2,\alpha}(\partial\Omega) \supset B_\varepsilon(0) \rightarrow \mathbb{C}$, mapping

$$\psi : f \mapsto \langle \Lambda_q(f), 1 \rangle_{L^2(\partial\Omega)} = \int_{\partial\Omega} \Lambda_q(f) dS_x. \quad (15)$$

Following [23], we call ψ a *measurement function*.

Remark 4.2. Some care is required when making numerical differences of the type $u_+ - u_-$, to avoid canceling significant digits. This is already visible at the level of the corresponding Calderón exponentials. Let $v_1 = e^{(\zeta+i\xi)\cdot x/2}$ and $v_2 = e^{(-\zeta+i\xi)\cdot x/2}$, and denote $s = \zeta \cdot x$. Then

$$(v_1 + v_2)^2 = e^{i\xi\cdot x} (e^s + e^{-s})^2 = e^{i\xi\cdot x} 4 \cosh^2(s),$$

and

$$(v_1 - v_2)^2 = e^{i\xi\cdot x} (e^s - e^{-s})^2 = e^{i\xi\cdot x} 4 \sinh^2(s).$$

For $|s| \gg 1$ we have

$$\cosh^2(s), \sinh^2(s) \sim \frac{1}{4}e^{2|s|},$$

so each individual quantity $(v_1 \pm v_2)^2$ is of magnitude $\sim e^{2|s|}$, while their difference

$$(v_1 + v_2)^2 - (v_1 - v_2)^2 = 4e^{i\xi\cdot x}$$

remains $O(1)$. Thus, the relative size of the difference compared to the operands is approximately

$$\frac{|(v_1 + v_2)^2 - (v_1 - v_2)^2|}{\max\{|(v_1 + v_2)^2|, |(v_1 - v_2)^2|\}} \approx 4e^{-2|s|},$$

which becomes smaller than machine precision when $|s|$ is too large. In our numerical experiments, we ensure numerical stability by choosing ζ and the computational grid so that $4e^{-2|\zeta\cdot x|} \geq 2.22 \times 10^{-16}$, which is satisfied by imposing $|\zeta \cdot x| \leq 18.7$ (we use the more comfortable bound $|\zeta \cdot x| \leq 10$) on the computational domain.

We also mention that purely real boundary values can also be used. The technique is analogous to those above, so we only briefly outline the strategy. Consider

$$\begin{cases} -\Delta u + q u^2 = 0, & x \in \Omega, \\ u = \varepsilon_1 f_1 + \varepsilon_2 f_2, & x \in \partial\Omega. \end{cases}$$

Now it can be seen that the first linearizations $v_j := D_\varepsilon u|_{\varepsilon_1=\varepsilon_2=0}$ in Ω , $j = 1, 2$, are harmonic with the Dirichlet boundary values f_j . The second linearizations $w_\alpha = D_{\varepsilon_1, \varepsilon_2}^\alpha u|_{\varepsilon_1=\varepsilon_2=0}$ with the multi-index $\alpha \in \mathbb{N}^2$ with $|\alpha| = 2$ satisfy $-\Delta w_\alpha + 2q v_1^{\alpha_1} v_2^{\alpha_2} = 0$ in Ω with zero Dirichlet boundary values. Therefore, the solution w to $-\Delta w + 2q v^2 = 0$ in Ω , where v is harmonic with complex boundary value f , can be obtained from real boundary values $f_1 = \Re(f)$ and $f_2 = \Im(f)$ as the linear combination

$$w = w_{(2,0)} + 2iw_{(1,1)} - w_{(0,2)}.$$

This argument holds in general with power-type nonlinearities.

4.2 Numerical reconstruction of the potential from its Fourier transform

We embed the computation domain $\Omega \subset \mathbb{R}^2$ into an axis-aligned rectangle, for $(N_x, N_y) \in \mathbb{N}^2$ denoting the numbers of cells in x and y directions, we define

$$B = [x_{\min}, x_{\min} + N_x h] \times [y_{\min}, y_{\min} + N_y h] \quad \text{with} \quad \bar{\Omega} \subset B,$$

and first construct a uniform Cartesian mesh of B by square cells $\{p_{m,n}\}$ of side $h > 0$. Each cell is

$$\begin{aligned} p_{m,n} &= [x_m, x_{m+1}] \times [y_n, y_{n+1}] \\ &= [x_{\min} + mh, x_{\min} + (m+1)h] \times [y_{\min} + nh, y_{\min} + (n+1)h] \end{aligned} \quad (16)$$

with

$$(m, n) \in \{0, \dots, N_x - 1\} \times \{0, \dots, N_y - 1\}.$$

We then restrict the reconstruction grid to Ω , retaining only the cells whose centers

$$c_{m,x} := x_{\min} + \left(m + \frac{1}{2}\right)h, \quad c_{n,y} := y_{\min} + \left(n + \frac{1}{2}\right)h$$

satisfy $(c_{m,x}, c_{n,y}) \in \Omega$. The number of pixels retained is then $N' = N'_x \times N'_y$, in obvious notation. Removing cells outside Ω reduces the size of the linear system later on and prevents the inversion from reconstructing non-physical mass outside of Ω , which might degrade the reconstruction.

Next, approximate a (complex-valued) $f: \Omega \rightarrow \mathbb{C}$ by a piecewise constant function over each cell using the basis expansion:

$$\mathbf{f}(X) = \sum_{m,n} f_{m,n} \varphi_{m,n}(X),$$

where the indicator basis functions $\varphi_{m,n}$ are defined by

$$\varphi_{m,n}(X) = \begin{cases} 1, & \text{if } X \in p_{m,n}, \\ 0, & \text{otherwise.} \end{cases}$$

To compute the Fourier transform of f , we evaluate the contribution of each cell $p_{m,n}$ at a discrete set of frequencies $\xi_k \in \mathbb{R}^2$, resulting in the expression

$$\widehat{f}(\xi_k) = \int_{p_{m,n}} f(X) e^{-i\xi_k \cdot X} dX = \sum_{m,n} f_{m,n} \int_{p_{m,n}} e^{-i\xi_k \cdot X} dX.$$

For isotropic resolution, we sample the frequency points ξ_k in polar coordinates, that is,

$$\xi_k = (r_\ell \cos \theta_j, r_\ell \sin \theta_j) = (\xi_{k,x}, \xi_{k,y}), \quad (17)$$

where $r_\ell \in [0, R_{\max}]$ denotes the radial coordinate and $\theta_j \in [0, 2\pi)$ the angular coordinate; here $\xi_{k,x}$ and $\xi_{k,y}$ denote the corresponding Cartesian components. We choose a finite number of radii N_r and angles N_θ , producing a total of $N_r \times N_\theta$ sampling points that form a polar grid in the Fourier domain.

We next build the matrix $E \in \mathbb{C}^{K \times N'}$, where $N' = N'_x \times N'_y$ and $K = N_r \times N_\theta$, and whose entries $E_{(k_x, k_y), (m, n)}$ represent the contribution of the cell $p_{m,n}$ to the Fourier coefficient associated with frequency ξ_k

If $\xi_{k,x} \neq 0$ and $\xi_{k,y} \neq 0$

$$\begin{aligned} E_{(k_x, k_y), (m, n)} &= \int_{x_m}^{x_{m+1}} \int_{y_n}^{y_{n+1}} e^{-i(\xi_{k,x}x + \xi_{k,y}y)} dy dx \\ &= \frac{-1}{\xi_{k,x}\xi_{k,y}} (e^{-i\xi_{k,x}h} - 1) (e^{-i\xi_{k,y}h} - 1) e^{-i(\xi_{k,x}x_m + \xi_{k,y}y_n)}, \end{aligned}$$

where $x_m = x_{min} + mh$ and $y_n = y_{min} + nh$, so

$$E_{(k_x, k_y), (m, n)} = h^2 \operatorname{sinc}\left(\frac{1}{2}\xi_{k_x} h\right) \operatorname{sinc}\left(\frac{1}{2}\xi_{k_y} h\right) e^{-i(\xi_{k_x} c_{m,x} + \xi_{k_y} c_{n,y})}$$

where the function $\operatorname{sinc}(t) = \frac{\sin(t)}{t}$, with the continuous limit $\operatorname{sinc}(t) = 1$ at $t \rightarrow 0$ is used in the numerical implementation for stability.

If $\xi_{k_x} = 0$ (or $\xi_{k_y} = 0$ by symmetry),

$$E_{(k_x, k_y), (m, n)} = h^2 e^{-i\xi_{k_y} c_{n,y}} \operatorname{sinc}\left(\frac{1}{2}\xi_{k_y} h\right),$$

Else,

$$E_{(k_x, k_y), (m, n)} = h^2.$$

To simplify notation and enable matrix computations, we flatten the two dimensional indices (m, n) (resp. (k_x, k_y)) into a single global index $I \in \{0, \dots, N' - 1\}$ (resp. $K \in \{0, \dots, K_r K_\theta - 1\}$) using row-major ordering:

$$I = n \cdot N_x + m \quad (\text{resp.} \quad K = k_r \cdot K_\theta + k_\theta)$$

The discrete Fourier transform vector $F \in \mathbb{C}^K$ can then be approximated as:

$$F_k \approx \sum_{I=0}^{N'-1} E_{k,I} q_I,$$

or in matrix form,

$$F = Eq, \tag{18}$$

where $q \in \mathbb{C}^{N'}$ contains the piecewise constant values $q_I = q_{m,n}$, and $F \in \mathbb{C}^K$ represents the approximated Fourier coefficients of q at the frequencies ξ_k .

Remark 4.3. If the potential function q in (2) is known to be real-valued then, since $\widehat{q}(-\xi) = \overline{\widehat{q}(\xi)}$, it suffices to use frequency components in the upper half-plane $\xi_y \geq 0$ by taking, for example, $\theta_j \in [0, \pi)$ above.

We finally touch on the choice of the bandwidth R_{\max} of frequencies ξ and the discretization width h of the reconstruction grid of q . We choose $N' \geq K$, so that the system $Eq = F$ is under-determined. The usual Nyquist rule suggests that one can expect good resolution reconstructions in fairly coarse grids with $h \sim \pi/R_{\max}$. However, in practise, we choose much finer discretization ($h \ll \pi/R_{\max}$) and suppress the arising small singular values (see Figure 1, below) of E via regularization strategies, such as Tikhonov or TV-regularization, using a priori information about the smoothness of the potential q .

4.3 Reconstruction of the potential from noisy measurements

In practice, measurement data are inevitably contaminated by noise. We model this by adding synthetic complex Gaussian noise to the measured Fourier data. The noise level is chosen relative to the maximum absolute value of the measurements.

The measurement is

$$\int_{\partial\Omega} \partial_\nu (u_+ - u_-)_\varepsilon ds + \eta(\xi) \tag{19}$$

where $\eta(\xi)$ denotes an additive complex Gaussian noise term associated with the Fourier mode $\xi \in \mathbb{R}^2$. Here, ξ represents the spatial frequency variable in the Fourier domain, and the random process $\eta(\xi)$ models independent noise realizations for each frequency component.

When finite-difference schemes are employed to approximate the second derivative with respect to ε in equation (13), the reconstruction becomes highly unstable in the presence of noise [7]. This instability arises because finite differences amplify measurement errors, leading to poor recovery of the potential $q(x)$. To overcome this limitation, we instead employ more robust differentiation strategy, Savitzky-Golay (see appendix B) which provide greater noise tolerance while preserving essential features of the signal.

In the numerical reconstructions of Section 5, we employ the Savitzky-Golay filter (originally introduced in the chemistry literature for smoothing noisy spectra [33]) to smooth the data. The method consists of fitting, on each sliding window of odd length $2m+1$, a local polynomial of degree p by least squares and, in our case, evaluating its derivatives at the window center for numerical differentiation (For further details, see Appendix B). We also tested spline-based smoothing, which yielded competitive results, but we omit those reconstructions here for brevity and because Savitzky-Golay requires fewer tuning parameters in our setup.

To recover the potential q from the discrete linear system (18), we employ regularization techniques that stabilize the inversion and reduce the effects of noise and ill-conditioning. The rapid decay of the singular values (see Fig. 1) clearly shows that recovering the potential from Fourier data is a severely ill-posed problem, which justifies the use of Tikhonov or TV regularisation.

Depending on the expected regularity of the underlying potential, we consider two complementary approaches: Tikhonov regularization, suitable for smoothly varying potentials, and Total Variation (TV) regularization, designed for piecewise-smooth or discontinuous potentials. Also, if it is known that recovery of particular frequencies (such as low frequencies) is more stable, this might be used in the regularization strategy. For example, one might use different regularization parameters for low and high frequencies, respectively.

Tikhonov regularization To stably recover the unknown vector $q \in \mathbb{R}^N$ from the possibly ill-posed linear system $Eq = F$, we apply Tikhonov regularization, which introduces a penalization term to enforce stability and incorporate prior knowledge about the solution. The regularized estimate q_λ is obtained as the solution to the minimization problem

$$q_\lambda = \arg \min_{q \in \mathbb{R}^N} \{ \|Eq - F\|_2^2 + \lambda \|\Gamma q\|_2^2 \},$$

where $\lambda > 0$ is the regularization parameter, and $\Gamma \in \mathbb{R}^{K \times N}$ is a regularization operator that typically encodes smoothness (e.g., identity or a discrete derivative matrix). In our setting, we take

$$\Gamma = [\text{Id}, D_x, D_y].$$

where D_x (resp. D_y) denotes the discrete derivative operator in the x -direction (resp. in the y -direction).

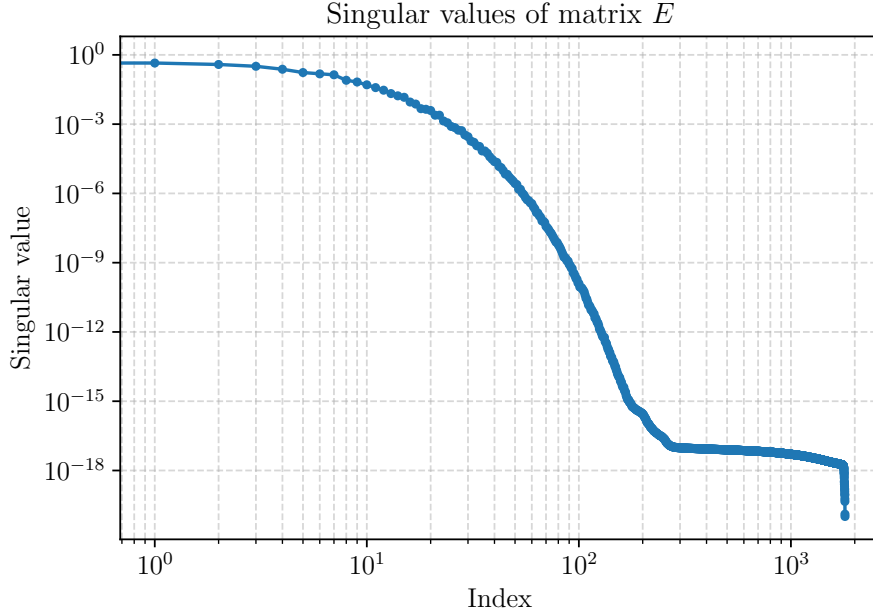


Figure 1: Singular values of the Fourier matrix $E \in \mathbb{C}^{1800 \times 17692}$ in log-log scale ($N_r = 60$, $N_\theta = 30$, $N_x = N_y = 150$).

The minimizer q_λ satisfies the normal equations:

$$(E^\top E + \lambda \Gamma^\top \Gamma) q_\lambda = E^\top F.$$

This formulation ensures a stable and well-posed solution even when the original system $Eq = F$ is ill-conditioned.

Total Variation (TV) regularization To promote reconstructions that are piecewise smooth and preserve sharp edges, we employ Total Variation (TV) regularization. Given the ill-posed linear system $Eq = F$, the TV-regularized estimate q_λ is defined as the minimizer of the variational problem

$$q_\lambda = \arg \min_{q \in \mathbb{R}^N} \{ \|Eq - F\|_2^2 + \lambda \text{TV}(q) \},$$

where $\lambda > 0$ controls the trade-off between data fidelity and regularity, and the TV semi-norm is given by

$$\text{TV}(q) = \sum_i (|\partial_x q_i| + |\partial_y q_i|).$$

Unlike the quadratic penalization in Tikhonov regularization, the TV penalty is non-smooth, which allows it to preserve discontinuities in q (such as edges in images or jumps in piecewise-constant potentials). This makes TV particularly effective in inverse problems where the true potential is expected to be sparse in its gradient. TV regularization is implemented using a quadratic optimization approach, following the methodology described in [35].

5 Numerical examples

In this section, we present several numerical experiments illustrating the reconstruction of the potential $q(x)$ from noisy boundary measurements, based on higher order

linearization method described in Section 2 that allows the recovery of q from the 2nd linearization of the measurement function ψ in (15), outlined in Sections 4.2 and 4.3. We experimented also on varying v_0 and using Calderón exponentials v . This produces qualitatively similar reconstructions and slightly simpler implementation, but for conciseness these results are not included here. The experiments are designed to test different smoothness assumptions on q .

5.1 Computational setup

All simulations were run on *Lehmus*, the University of Oulu’s (Finland) high performance computing cluster. Each job used 64 CPU cores. The wall clock time is dominated by the forward solver; once the measurement data are available, the inverse reconstruction is comparatively fast, particularly with Tikhonov regularization.

The forward problems is implemented using the **FEniCSx** framework for finite element discretization and nonlinear solvers based on Newton’s method as shown in Section 3. All simulations are performed in two spatial dimensions on a circular domain (but the choice of domains of other shapes is also possible)

$$\Omega = \{(x, y) \in \mathbb{R}^2 : x^2 + y^2 \leq 1\},$$

with Dirichlet boundary conditions. The synthetic DN-map is simulated by evaluating

$$\Lambda_q(f) = (n_x \cdot \nabla u)|_{\partial\Omega},$$

where n_x is the outward pointing unit normal vector of $\partial\Omega$ at x .

In all numerical experiments, the measurement data are corrupted by additive complex Gaussian noise to emulate realistic experimental uncertainty as shown in (19). The measurement, i.e. the integral from (19) with a finite parameter ε_k , is denoted by

$$I(\varepsilon_k) := \int_{\partial\Omega} \partial_\nu(u_+ - u_-)_{\varepsilon_k} ds.$$

We define the noisy data as

$$I_{\text{noisy}}(\varepsilon_k) = I(\varepsilon_k) + \sigma(\eta_{1,k} + i\eta_{2,k}),$$

where $\eta_{1,k}, \eta_{2,k} \sim \mathcal{N}(0, 1)$ are independent standard normal random variables, and the noise amplitude is scaled according to

$$\sigma = \rho \max_{\varepsilon_k} |I(\varepsilon_k)|,$$

with $\rho > 0$ representing the prescribed relative noise level. In the examples presented below, we fix the noise level to $\rho = 0.01$, corresponding to 1% relative Gaussian noise, which gives an average signal-to-noise ratio of approximately 29.24 dB.

The second derivative with respect to the perturbation parameter ε is approximated using a Savitzky–Golay polynomial filter with $N_\varepsilon = 64$ sampling points uniformly distributed in $\varepsilon \in [-2, 2]$ and a smoothing window of size `window = 51`.

For the Tikhonov method, the regularization parameter is chosen experimentally and fixed to $\lambda = 10^{-10}$ in Examples 5.2 and 5.2, while for TV method we use

$\lambda = 10^{-7}$ in Example 5.2 and $\lambda = 10^{-6}$ in Example 5.2. The computational grid consists of $N_x = N_y = 150$ nodes in each spatial direction.

The Fourier data are sampled on a polar grid as explained in 17. In the experiments, we take $N_r = 60$ radial samples and $N_\theta = 30$ angular directions, with maximum radius $R_{\max} = 5.0$, resulting in quite limited bandwidth measurements.

In summary, the reconstruction of q_{rec} reduces to the following regularized problem:

$$q_{\text{rec}} = \arg \min_q \frac{1}{2} \left\| \underbrace{(\mathcal{D}_{\text{SG}}^2 I_{\text{noisy}})(0)}_{\text{SG 2nd derivative of } I \text{ at } \varepsilon=0} - Eq \right\|_2^2 + \lambda \mathcal{R}(q),$$

with the regularizer chosen according to the desired features,

$$\mathcal{R}(q) \in \{ \|q\|_{L^2(\Omega)}^2 \text{ (Tikhonov)}, \text{TV}(q) \text{ (TV)} \}.$$

5.2 Test potentials

To assess reconstruction accuracy under different regularity regimes, we consider several synthetic test potentials $q(x, y)$ ranging from smooth to piecewise constant with jump discontinuities.

Example 1. Smooth, localized bump.

Define the smooth, compactly supported profile

$$\varphi(x; d) = \begin{cases} \exp\left(\frac{1}{\left|\frac{x}{d}\right|^2 - 1} + 1\right), & |x| < d, \\ 0, & \text{otherwise,} \end{cases}$$

where $d > 0$ sets the characteristic width. Using this profile, we build a radially symmetric potential centered at (x_0, y_0) by

$$q(x, y; x_0, y_0, d) := \varphi\left(\sqrt{(x - x_0)^2 + (y - y_0)^2}; d\right).$$

Figure 2 reports results for a centered bump at $(0, 0)$. Panel 2a shows the real part of the Fourier transform of the potential: the reconstruction from boundary data is displayed next to the exact Fourier data. Panel 2b presents the spatial reconstruction alongside the ground truth; the location and shape of the bump are captured accurately.

Figure 3 reports the off-center bump case, located at $(0.2, 0.4)$. Panel 3a displays, side by side, the real part of the exact and reconstructed Fourier transform. Panel 3b shows the reconstructed potential next to the ground truth; the displacement from the origin and overall shape are recovered effectively.

Example 2. Superposition of two bumps.

To introduce mild asymmetry and multiple peaks, we also consider a sum of two localized bumps:

$$q(x, y; x_0, y_0, d) = \varphi\left(\sqrt{(x - x_0)^2 + (y - y_0)^2}; d\right) + \frac{1}{2} \varphi\left(\sqrt{(x + 2x_0)^2 + (y + y_0)^2}; d\right).$$

The results are shown in Figure 4 and demonstrate a good reconstruction of the two bumps, even with different sizes and amplitudes.

Example 3. Discontinuous annulus (ring). Let χ_O be the indicator of the open annulus

$$O = \{(x, y) \in \Omega : R_{\text{in}} < \sqrt{x^2 + y^2} < R_{\text{out}}\},$$

i.e.,

$$\chi_O(x, y; R_{\text{in}}, R_{\text{out}}) = \begin{cases} 1, & R_{\text{in}} < \sqrt{x^2 + y^2} < R_{\text{out}}, \\ 0, & \text{otherwise.} \end{cases}$$

and

$$q(x, y; R_{\text{in}}, R_{\text{out}}) = \chi_O(x, y; R_{\text{in}}, R_{\text{out}}).$$

Figure 5 shows the results for this example. The reconstruction, obtained with TV regularization, closely captures the sharp inner and outer edges, preserving the jump discontinuities at both radii.

Example 4. Discontinuous star shaped set. Define χ_S as the indicator of the star shaped region

$$S = \{(x, y) \in \Omega : \sqrt{x^2 + y^2} < R_0 + a \cos(k \theta(x, y))\},$$

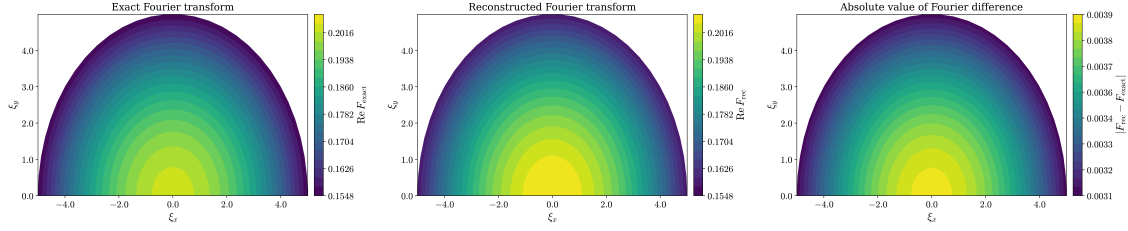
where $\theta(x, y) = \text{atan2}(y, x)$, and $R_0 > 0$, $a \in \mathbb{R}$, $k \in \mathbb{N}$:

$$\chi_S(x, y; R_0, a, k) = \begin{cases} 1, & \sqrt{x^2 + y^2} < R_0 + a \cos(k \theta(x, y)), \\ 0, & \text{otherwise.} \end{cases}$$

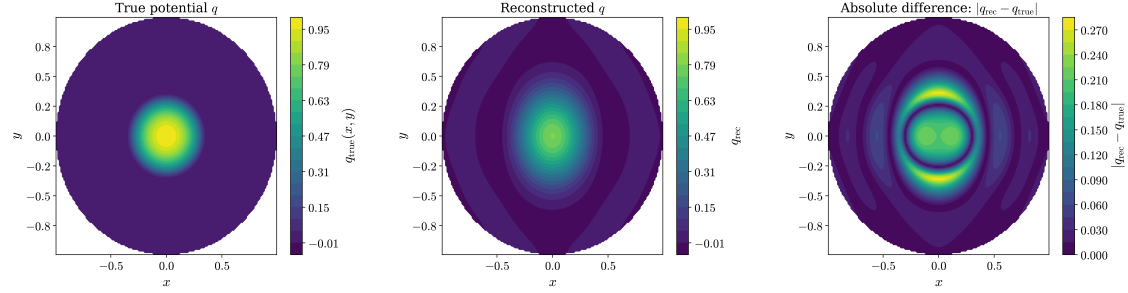
and

$$q(x, y; R_0, a, k) = \chi_S(x, y; R_0, a, k).$$

In Figure 6, the reconstruction obtained with TV regularization captures the overall star shaped contour; however, given the complexity of this geometry, the reconstruction does not fully recover the inner corners of the star.

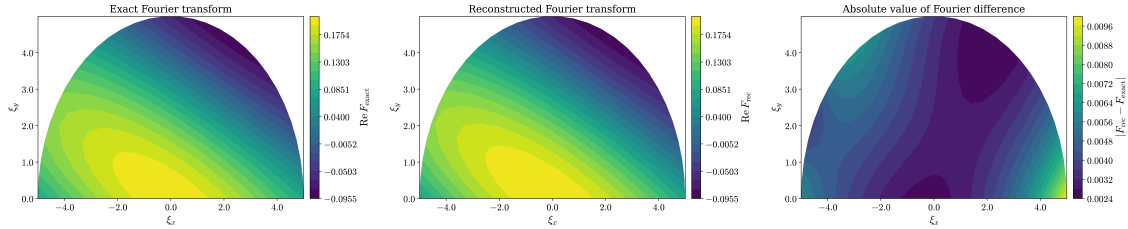


(a) Recovered real Fourier data $\Re \mathcal{F}(q)$ for the centered bump: exact Fourier transform computed via Gauss-Legendre quadrature (left), reconstruction from noisy boundary measurements (middle), and their difference (right).

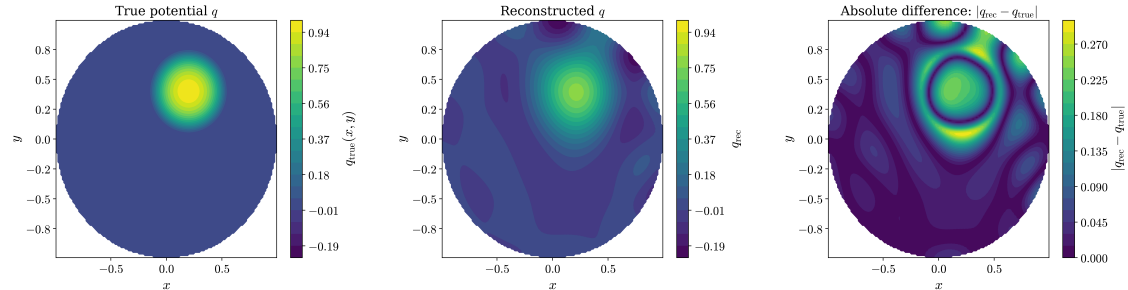


(b) Centered bump $q(x, y; 0, 0, 0.4)$: ground truth (left), reconstruction (middle), and residual (right). The reconstruction recovers the bump's location and amplitude well, the L^2 error is 0.127

Figure 2: Example 1: Smooth, localized bump (centered).



(a) Recovered real Fourier data $\Re \mathcal{F}(q)$ for the off center bump: exact Fourier transform computed via Gauss-Legendre quadrature (left), reconstruction from noisy boundary measurements (middle), and their difference (right).



(b) Off center bump $q(x, y; 0.2, 0.4, 0.4)$: ground truth (left), reconstruction (middle), and residual (right). Both the position and magnitude of the bump are well reproduced (L^2 error is 0.147)

Figure 3: Example 1: Smooth, localized bump (off center).

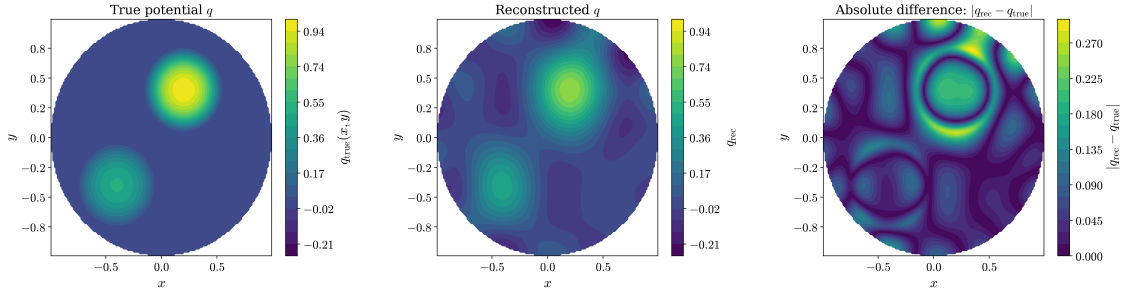


Figure 4: Example 2: Two bump potential $q(x, y; 0.2, 0.4, 0.4)$: ground truth (left), reconstruction (middle), and residual (right). The localization and width of the bumps are well reconstructed with Tikhonov regularization (L^2 error is 0.153)

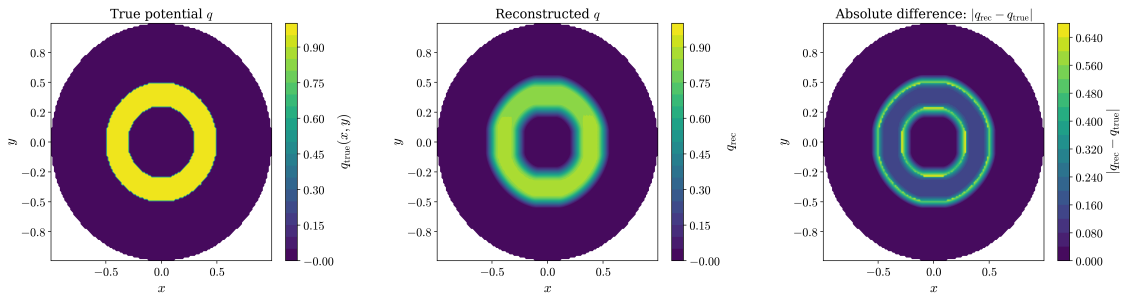


Figure 5: Example 3: Ring potential $q(x, y; 0.3, 0.5)$: ground truth (left), reconstruction (middle), and residual (right). The jump discontinuities are slightly blurred, but piecewise constantness is well-captured with TV regularization (L^2 error is 0.229).

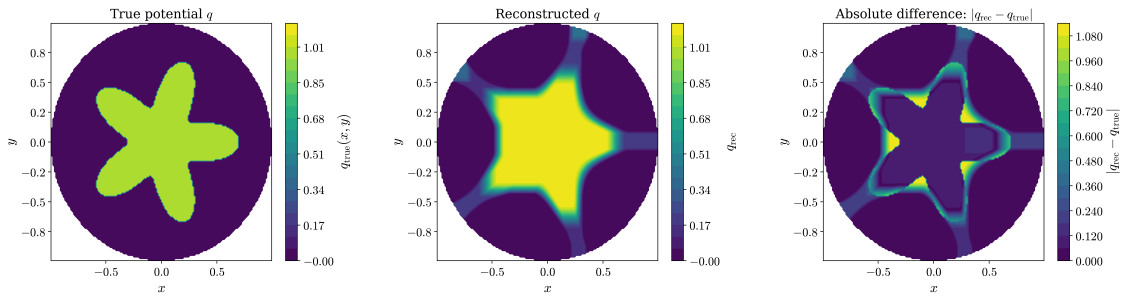


Figure 6: Example 4: Star shaped potential $q(x, y; 0.5, 0.2, 5)$: ground truth (left), reconstruction (middle), and residual (right). TV regularization recovers the star's overall shape and sharp edges, but it falls short at the inner corners due to the geometry's complexity.

Acknowledgements

K.E-M. and T.T. were supported by the Finnish Ministry of Education and Culture's Pilot for Doctoral Programmes (Pilot project Mathematics of Sensing, Imaging and Modelling), the Research Council of Finland (Flagship of Advanced Mathematics for Sensing Imaging and Modelling grant 359186), and Emil Aaltonen foundation. M.L. was supported by a AdG project 101097198 of the European Research

Council, Centre of Excellence of Research Council of Finland, and the FAME flagship of the Research Council of Finland (grant 359182). Views and opinions expressed are those of the authors only and do not necessarily reflect those of the European Union or the other funding organizations. The European Union can not be held responsible for them.

A Justification of the Newton method

To apply the Lax-Milgram theorem, we use standard tools to establish the boundedness and coercivity of the sesquilinear form (8). So, let $\Omega \subset \mathbb{R}^d$ be a bounded Lipschitz domain.

We first show that the linear operator $F(u_n) : V \rightarrow \mathbb{C}$ defined in (6) is continuous; that is, for any fixed $u_n \in V$, there exists a constant $C(n) > 0$ such that

$$|F(u_n)(v)| \leq C(n) \|v\|_{H^1(\Omega)} \quad \text{for all } v \in V.$$

Indeed, by Cauchy-Schwarz inequality and the Sobolev embedding $H^1(\Omega) \subset L^q(\Omega)$ for any $1 \leq q < \infty$ (due to boundedness of Ω) we have

$$\begin{aligned} |F(u_n)(v)| &\leq \|\nabla u_n\|_{L^2(\Omega)} \|\nabla v\|_{L^2(\Omega)} + \|q\|_{L^\infty(\Omega)} \|u_n^p\|_{L^2(\Omega)} \|v\|_{L^2(\Omega)} \\ &\leq \|\nabla u_n\|_{L^2(\Omega)} \|\nabla v\|_{L^2(\Omega)} + \|q\|_{L^\infty(\Omega)} \|u_n\|_{L^{2p}(\Omega)}^p \|v\|_{L^2(\Omega)} \\ &\leq (\|\nabla u_n\|_{L^2(\Omega)} + \|q\|_{L^\infty(\Omega)} C_1 \|u_n\|_{H^1(\Omega)}^p) \|v\|_{H^1(\Omega)} \\ &\leq C(n) \|v\|_{H^1(\Omega)}, \end{aligned}$$

with $C(n) = \|\nabla u_n\|_{L^2(\Omega)} + \|q\|_{L^\infty(\Omega)} C_1 \|u_n\|_{H^1(\Omega)}^p$. Hence, $F(u_n)$ defines a bounded conjugate linear functional $V \rightarrow \mathbb{C}$.

To establish the boundedness of $J(u_n; \cdot, \cdot)$ we, similarly as above, apply Cauchy-Schwarz, generalized Hölder inequality, Poincaré inequality, and the Sobolev embeddings $H^1(\Omega) \hookrightarrow L^3(\Omega)$ and $H^1(\Omega) \hookrightarrow L^{3(p-1)}(\Omega)$:

$$\begin{aligned} |J(u_n; u, v)| &\leq \left| \int_{\Omega} \nabla u \cdot \nabla \bar{v} \, dx \right| + \left| \int_{\Omega} p q(x) u_n^{p-1} u \bar{v} \, dx \right| \\ &\leq \|\nabla u\|_{L^2(\Omega)} \|\nabla v\|_{L^2(\Omega)} + p \|q\|_{L^\infty(\Omega)} \|u_n^{p-1}\|_{L^3(\Omega)} \|u\|_{L^3(\Omega)} \|v\|_{L^3(\Omega)} \\ &\leq \|\nabla u\|_{L^2(\Omega)} \|\nabla v\|_{L^2(\Omega)} + p \|q\|_{L^\infty(\Omega)} \|u_n\|_{L^{3(p-1)}(\Omega)}^{p-1} \|u\|_{L^3(\Omega)} \|v\|_{L^3(\Omega)} \\ &\leq \|u\|_{H^1(\Omega)} \|v\|_{H^1(\Omega)} + C_0 p \|q\|_{L^\infty(\Omega)} \|u_n\|_{H^1(\Omega)}^{p-1} \|u\|_{H^1(\Omega)} \|v\|_{H^1(\Omega)} \\ &\leq \left(1 + C_0 p \|q\|_{L^\infty(\Omega)} \|u_n\|_{H^1(\Omega)}^{p-1} \right) \|u\|_{H^1(\Omega)} \|v\|_{H^1(\Omega)}. \end{aligned}$$

Here $C_0 > 0$ is a generic constant depending only on Ω and the Sobolev embeddings $H^1(\Omega) \hookrightarrow L^3(\Omega)$ and $H^1(\Omega) \hookrightarrow L^{3(p-1)}(\Omega)$ used in the estimate.

Finally, to prove the coercivity of $J(u_n; \cdot, \cdot)$ we estimate using the Sobolev em-

bedding and Poincaré inequality

$$\begin{aligned}
|J(u_n; u, u)| &\geq \left| \int_{\Omega} \nabla u \cdot \nabla \bar{u} \, dx \right| - \left| \int_{\Omega} pq(x) u_n^{p-1} u \bar{u} \, dx \right| \\
&\geq \|\nabla u\|_{L^2(\Omega)}^2 - p\|q\|_{L^\infty(\Omega)} \|u_n^{p-1}\|_{L^2(\Omega)} \|u^2\|_{L^2(\Omega)} \\
&= \|\nabla u\|_{L^2(\Omega)}^2 - p\|q\|_{L^\infty(\Omega)} \|u_n\|_{L^{2(p-1)}(\Omega)}^{p-1} \|u\|_{L^4(\Omega)}^2 \\
&\geq C_2 \|u\|_{H^1(\Omega)}^2 - C_3 p \|q\|_{L^\infty(\Omega)} \|u_n\|_{H^1(\Omega)}^{p-1} \|u\|_{H^1(\Omega)}^2 \\
&= C_2 \left(1 - \frac{C_3}{C_2} p \|q\|_{L^\infty(\Omega)} \|u_n\|_{H^1(\Omega)}^{p-1}\right) \|u\|_{H^1(\Omega)}^2 \\
&\geq \beta_n \|u\|_{H^1(\Omega)}^2
\end{aligned}$$

Above we used a single constant C_3 to represent the Sobolev embedding constants controlling $\|u_n\|_{L^{2(p-1)}(\Omega)}$ and $\|u\|_{L^4(\Omega)}$ by $\|\cdot\|_{H^1(\Omega)}$, while C_2 denotes the constant arising from Poincaré's inequality.

Note $\beta_n > 0$ if

$$\|u_n\|_{H^1(\Omega)}^{p-1} < \frac{C_2}{C_3 p \|q\|_{L^\infty(\Omega)}}.$$

Thus $J(u_n; \cdot, \cdot)$ is bounded coercive sesquilinear form if $u_n \in V$ is sufficiently small. Since $F(u)$ is linear and bounded, the Lax-Milgram theorem applies and the Newton iteration is justified.

Remark A.1. We recall the standard Newton-Kantorovich convergence result (see Chapter 12, Theorem 12.6.2 of [28]). We have that the Fréchet derivative $DF(u) = J(u)$ satisfies:

1. Bound on the inverse,

$$\|J(u_n)^{-1}\|_{\mathcal{L}(V^*, V)} \leq M,$$

this follows from Lax-Milgram theorem that implies that $J(u_n)$ is invertible and that $\|J(u_n)^{-1}\|_{\mathcal{L}(V^*, V)} \leq \beta_n^{-1}$, provided that

$$\|u_n\|_{H^1(\Omega)}^{p-1} \leq \frac{C_2}{C_3 p \|q\|_{L^\infty(\Omega)} + 1}.$$

2. Lipschitz condition in a neighbourhood of the solution u ,

$$\|J(u_n) - J(u)\|_{\mathcal{L}(V, V^*)} \leq L \|u_n - u\|_{H^1}.$$

This property follows from the fact that the nonlinearity $w \mapsto w^{p-1}$ is Lipschitz on bounded sets together with the boundedness of q and the Sobolev embeddings in two dimensions.

Let u be the exact solution of $F(u) = 0$ and let (u_n) be the Newton iterates

$$u_{n+1} = u_n - J(u_n)^{-1} F(u_n).$$

A Taylor expansion with integral remainder yields

$$F(u_n) = J(u)e_n + R_n, \quad e_n := u_n - u,$$

with

$$\|R_n\|_{V^*} \leq \frac{L}{2} \|e_n\|_V^2.$$

Using the Newton update and the above properties of J , one obtains the classical estimate

$$\|e_{n+1}\|_V \leq ML \|e_n\|_V^2 + \frac{ML}{2} \|e_n\|_V^2 = \frac{3ML}{2} \|e_n\|_V^2,$$

which shows quadratic convergence as long as the iterates remain in the neighbourhood where the assumptions are valid.

B Savitzky-Golay regularized higher order differentiation as local polynomial regression

Let $\{(x_i, y_i)\}_{i=1}^N$ be samples of a (possibly complex valued) function $f : \mathbb{R} \rightarrow \mathbb{C}$ observed with additive noise:

$$y_i = f(x_i) + \varepsilon_i, \quad \mathbb{E}[\varepsilon_i] = 0, \quad \text{Var}(\varepsilon_i) = \sigma^2. \quad (20)$$

Assume a uniform grid $x_i = x_0 + i \Delta x$. The Savitzky-Golay (SG) method [30, 33, 34] estimates the r -th derivative $f^{(r)}(x_i)$ by fitting, in a small moving window of $2m + 1$ points around x_i , a polynomial of degree $p \geq r$ via least squares, and then differentiating the fitted polynomial analytically at the window center. This is equivalent to applying a finite impulse response (FIR) convolution filter whose coefficients depend only on (p, r, m) and the spacing Δx .

Fix an index i and an odd window of $2m + 1$ points,

$$\mathcal{I}_i = \{i - m, \dots, i - 1, i, i + 1, \dots, i + m\}.$$

Introduce centered coordinates $t_j = x_{i+j} - x_i = j \Delta x$ for $j = -m, \dots, m$, and approximate f on the window by a degree- p polynomial g of the form

$$g(t) = \sum_{k=0}^p \beta_k t^k. \quad (21)$$

The coefficients β_0, \dots, β_p are determined by a least-squares fit to the noisy data $\{y_{i+j}\}_{j=-m}^m$, by solving

$$(\beta_0, \dots, \beta_p) = \arg \min_{\gamma_0, \dots, \gamma_p} \sum_{j=-m}^m |\gamma_0 + \gamma_1 t_j + \dots + \gamma_p t_j^p - y_{i+j}|^2.$$

The value of the fitted polynomial at the window center is $g(0) = \beta_0$, and its r -th derivative at $t = 0$ is given analytically by

$$g^{(r)}(0) = r! \beta_r.$$

Thus the SG estimate of $f^{(r)}(x_i)$ is obtained by locally replacing the noisy data with its best-fitting degree- p polynomial and evaluating its analytic derivative at the center of the window.

References

- [1] K. Astala and L. Päivärinta. Calderón’s inverse conductivity problem in the plane. *Annals of Mathematics*, pages 265–299, 2006.
- [2] T. Brander, B. Harrach, M. Kar, and M. Salo. Monotonicity and enclosure methods for the p -Laplace equation. *SIAM Journal on Applied Mathematics*, 78(2):742–758, 2018.
- [3] P. Caro, M. A. Garcia-Ferrero, and K. M. Rogers. Reconstruction for the calderón problem with lipschitz conductivities. *Analysis & PDE*, 18(8):2033–2060, 2025.
- [4] P. Caro and K. M. Rogers. Global uniqueness for the calderón problem with lipschitz conductivities. In *Forum of Mathematics, Pi*, volume 4, page e2. Cambridge University Press, 2016.
- [5] C. Cârstea, T. Liimatainen, and L. Tzou. The calderón problem on riemannian surfaces and of minimal surfaces. *arXiv preprint arXiv:2406.16944*, 2024.
- [6] S. Chandrasekhar. *An introduction to the study of stellar structure*. University of Chicago Press, 1939.
- [7] J. Cullum. Numerical differentiation and regularization. *SIAM Journal on Numerical Analysis*, 8(2):254–265, 1971.
- [8] J. S. Dokken. Fenicsx tutorial. <https://jsdokken.com/dolfinx-tutorial/chapter4/newton-solver.html>.
- [9] D. A. Frank-Kamenetskii. *Diffusion and heat transfer in chemical kinetics*. Plenum Press, 1969.
- [10] B. Gidas, W.-M. Ni, and L. Nirenberg. Symmetry and related properties via the maximum principle. *Communications in Mathematical Physics*, 68:209–243, 1979.
- [11] K. T. Gkikas and P.-T. Nguyen. Semilinear elliptic equations involving power nonlinearities and hardy potentials with boundary singularities. *Proceedings of the Royal Society of Edinburgh Section A: Mathematics*, 155(3):993–1050, 2025.
- [12] B. Haberman and D. Tataru. Uniqueness in calderón’s problem with lipschitz conductivities. 2013.
- [13] V. Isakov. On uniqueness in inverse problems for semilinear parabolic equations. *Archive for Rational Mechanics and Analysis*, 124, 1993.
- [14] V. Isakov and A. I. Nachman. Global uniqueness for a two-dimensional semilinear elliptic inverse problem. *Transactions of the American Mathematical Society*, 347(9):3375–3390, 1995.
- [15] V. Isakov and J. Sylvester. Global uniqueness for a semilinear elliptic inverse problem. *Communications on Pure and Applied Mathematics*, 47(10):1403–1410, 1994.

- [16] D. Johansson, J. Nurminen, and M. Salo. Inverse problems for semilinear elliptic pde with a general nonlinearity $a(x, u)$. *arXiv preprint arXiv:2312.12196*, 2023.
- [17] D. Johansson, J. Nurminen, and M. Salo. Inverse problems for semilinear elliptic equations with low regularity. *arXiv preprint arXiv:2505.05278*, 2025.
- [18] H. Kang and G. Nakamura. Identification of nonlinearity in a conductivity equation via the Dirichlet-to-Neumann map. *Inverse Problems*, 18(4):1079–1088, 2002.
- [19] C. T. Kelley. *Iterative methods for linear and nonlinear equations*. Society for Industrial and Applied Mathematics (SIAM), Philadelphia, PA, 1995.
- [20] Y. Kian, H. Liu, L.-L. Wang, and G.-H. Zheng. Determination and reconstruction of a semilinear term from point measurements. *arXiv preprint arXiv:2411.09922*, 2024.
- [21] R.-Y. Lai and Y.-H. Lin. Global uniqueness for the fractional semilinear Schrödinger equation. *Proceedings of the American Mathematical Society*, 147(3):1189–1199, 2019.
- [22] M. Lassas, T. Liimatainen, Y.-H. Lin, and M. Salo. Inverse problems for elliptic equations with power type nonlinearities. *Journal de mathématiques pures et appliquées*, 145:44–82, 2021.
- [23] M. Lassas, T. Liimatainen, L. Potenciano-Machado, and T. Tyni. Uniqueness, reconstruction and stability for an inverse problem of a semi-linear wave equation. *J. Differ. Eq.*, 337:395–435, 2022.
- [24] T. Liimatainen, Y.-H. Lin, M. Salo, and T. Tyni. Inverse problems for elliptic equations with fractional power type nonlinearities. *Journal of Differential Equations*, 306:189–219, 2022.
- [25] J. D. Murray. *Mathematical biology I: An introduction*. Springer, 3rd edition, 2002.
- [26] A. I. Nachman. Global uniqueness for a two-dimensional inverse boundary value problem. *Annals of Mathematics*, pages 71–96, 1996.
- [27] A. Okubo and S. A. Levin. *Diffusion and ecological problems: modern perspectives*, volume 14 of *Interdisciplinary Applied Mathematics*. Springer, 2nd edition, 2001.
- [28] J. M. Ortega and W. C. Rheinboldt. *Iterative solution of nonlinear equations in several variables*. Society for Industrial and Applied Mathematics (SIAM), Philadelphia, PA, 1970.
- [29] C.-C. Pao. *Nonlinear parabolic and elliptic equations*. Plenum Press, New York, 1992.

- [30] W. H. Press, S. A. Teukolsky, W. T. Vetterling, and B. P. Flannery. *Numerical recipes in C: The art of scientific computing*. Cambridge University Press, 2 edition, 1992. See section 14.8.
- [31] F. Project. Dofinx api documentation. https://docs.fenicsproject.org/dofinx/v0.3.0/cpp/d9/dbf/classdofinx_1_1nls_1_1NewtonSolver.html.
- [32] M. Salo and X. Zhong. An inverse problem for the p -Laplacian: boundary determination. *SIAM Journal on Mathematical Analysis*, 44(4):2474–2495, 2012.
- [33] A. Savitzky and M. J. E. Golay. Smoothing and differentiation of data by simplified least squares procedures. *Analytical Chemistry*, 36(8):1627–1639, 1964.
- [34] R. W. Schafer. What is a Savitzky–Golay filter? *IEEE Signal Processing Magazine*, 28(4):111–117, 2011.
- [35] S. Siltanen, J. L. Mueller, and H. Lassi. *Linear and nonlinear inverse problems with practical applications*. SIAM, 2021.
- [36] J. Smoller. *Shock waves and reaction–diffusion equations*. Springer, 2nd edition, 1994.
- [37] Z. Sun. On a quasilinear inverse boundary value problem. *Mathematische Zeitschrift*, 221(2):293–305, 1996.
- [38] Z. Sun. An inverse boundary-value problem for semilinear elliptic equations. *Electronic Journal of Differential Equations*, (37):1–11, 2010.
- [39] Z. Sun and G. Uhlmann. Inverse problems in quasilinear anisotropic media. *American Journal of Mathematics*, 119(4):771–797, 1997.
- [40] J. Sylvester and G. Uhlmann. A global uniqueness theorem for an inverse boundary value problem. *Annals of mathematics*, pages 153–169, 1987.
- [41] G. Uhlmann. Electrical impedance tomography and Calderón’s problem. *Inverse Problems*, 25(12):123011, 2009.

E-mail addresses:

Khaoula El Maddah: khaoula.elmaddah@oulu.fi (corresponding author)

Matti Lassas: matti.lassas@helsinki.fi

Teemu Tyni: teemu.tyni@oulu.fi